PROCEEDINGS OF SCIENCE

Observation of a family of all-charm tetraquarks at CMS

Yilin Zhou,[a,*] **Xining Wang**[b,*] **and Liangliang Chen**[c,*]

[a] *Institute of Modern Physics, Fudan University, 220 Handan Road, Shanghai, China*

[b] *Department of Physics, Tsinghua University, 30 Shuangqing Road, Beijing, China*

[c] *School of Physics and Technology, Nanjing Normal University, 1 Wenyuan Road, Nanjing, China*

E-mail: yilin.zhou@cern.ch

Using 315 fb^{-1} of proton-proton collision data recorded by the CMS detector, which provides 3.6 times more $J/\psi J/\psi$ pairs than the Run 2 study, the CMS experiment reports the observation of three structures in the $J/\psi J/\psi$ to four-muon channel, named $X(6600)$, $X(6900)$, and $X(7100)$, each with a significance well above 5σ, confirming and extending the previous Run 2 results. Strong interference effects among these states, also exceeding 5σ, indicate that they share the same quantum numbers. A complementary search in the $J/\psi\psi(2S)$ channel identifies two structures consistent with $X(6900)$ and $X(7100)$. Assuming common quantum numbers for the three states, as suggested by the interference pattern, a spin–parity analysis favors a $J^{PC} = 2^{++}$ assignment, and hadrons with such high spins are rather rare. Together, these results support the interpretation of these states as a family of all-charm tetraquarks, favoring a diquark–antidiquark configuration with both diquarks in a spin-1 state and providing new insights into the dynamics of exotic resonances.

The 17th International Conference on Heavy Quarks and Leptons (HQL 2025)
15-19 September, 2025
Peking University, Beijing, China

[*]Speaker

https://pos.sissa.it/

PoS(HQL2025)050

1. Heavy-flavor exotic hadron states

In 1964, Gell-Mann[1] and Zweig[2] independently proposed that hadrons are composed of quarks (q), with mesons formed from quark–antiquark pairs ($q\bar{q}$) and baryons from quark triplets (qqq). They also noted that the same principles allow for tetraquark and pentaquark configurations, hinting at the possibility of "exotic" hadrons beyond the conventional $q\bar{q}$ and qqq structures.

In the light quark sector, light-quark exotic states remain elusive because their signals are obscured by overlapping resonances in experiments, and their non-perturbative dynamics make theoretical modeling challenging. In contrast, heavy-flavor exotic hadrons, containing charm or bottom quarks, are theoretically more tractable because the heavy quark masses provide a scale well above Λ_{QCD}, allowing more reliable predictions. The discovery of the $X(3872)$ [3] initiated a surge of interest in heavy-flavor exotics, leading to the observation of numerous XYZ states. Among them, the charmonium-like resonances $Z_c(3900)$ [4] and $Z_c(4430)$ [5] are particularly notable because they contain a charm–anticharm pair and carry electric charge, which provides a clear indication of a multiquark configuration. Moreover, fully-heavy exotic hadrons, composed entirely of charm or bottom quarks, offer a particularly promising system for theoretical exploration, as they are less affected by light-quark dynamics and can provide unique insights into the binding mechanisms of multiquark states.

2. Experimental status of all-charm tetraquarks

A major step forward came from the efforts of ATLAS, CMS, and LHCb in searching for tetracharm candidates in the $J/\psi J/\psi$ to four-muon decay channel with the Run 2 dataset. These searches have provided growing evidence for three all-charm tetraquark candidates, $X(6600)$, $X(6900)$, and $X(7100)$. The $X(6600)$ was first reported by CMS in 2024 with a local statistical significance approaching 8σ [6], and although not explicitly claimed by ATLAS or LHCb, both collaborations saw structure in the $J/\psi J/\psi$ mass spectrum [7, 8] that appears to be similar to $X(6600)$. The $X(6900)$, the first structure discovered by LHCb in 2020 [7], has been observed by all three experiments with global significances exceeding 5σ [6–8]. Evidence for $X(7100)$ remains less conclusive as CMS reported this structure with a local significance of 4.7σ (3.4σ globally), whereas LHCb noted a small excess around 7.2 GeV, but did not pursue it due to its low significance [7] and ATLAS has seen no evidence [8]. ATLAS has also conducted two searches for tetracharm states in the $J/\psi\psi(2S)$ decay mode [8, 9]. The $X(6900)$ was clearly observed with a significance well above 5σ, whereas the $X(7100)$ appeared at the 3σ level in one model in the first search using only $\psi(2S) \to \mu^+\mu^-$ decays [8], but was not confirmed in the second search, which also included $\psi(2S) \to J/\psi\pi^+\pi^-(J/\psi \to \mu^+\mu^-)$ decays [9].

Despite these significant achievements, several critical issues remain unresolved. The existence of the $X(7100)$ structure still requires firm confirmation. While all experiments favored fit models that incorporated quantum interference effects, the models themselves were inconsistent, and the observed interference lacked statistical significance. Moreover, the mass splittings among the three structures reported by CMS with Run 2 data exceed those typical of spin or orbital excitations [6], and the pattern of X masses follows a Regge trajectory, indicating that they may belong to a radially excited family [10]. Above all, the central question remains whether these structures are indeed tetraquarks, and if so, what their internal configuration is.

3. CMS $J/\psi J/\psi$ analysis with combined Run 2 and Run 3 dataset

The CMS updated analysis incorporates an additional 180 fb^{-1} of data from Run 3 (2022–2024) at $\sqrt{s}$ = 13.6 TeV, together with the 135 fb^{-1} collected during Run 2 (2016–2018) at $\sqrt{s}$ = 13 TeV [11]. The selection of $J/\psi J/\psi$ events follows the same criteria as the previous Run 2 study [6] and is applied to both Run 2 and Run 3 datasets. A two-dimensional fit of the dimuon masses yields $12\,622 \pm 165$ signal events in the 6–15 GeV $J/\psi J/\psi$ mass range for Run 2, increasing to $44\,936 \pm 692$ when combining Run 2 and Run 3 data. The Run 3 yield, about 2.5 times larger, benefits from a 33% increase in integrated luminosity and a significant improvement in trigger efficiency due to a new dimuon trigger in the parked dataset [12].

In the interference fit model, the three resonances, $X(6600)$, $X(6900)$, and $X(7100)$, are each modeled by a relativistic S-wave Breit-Wigner function, denoted as BW_1, BW_2, and BW_3, respectively. The background consists of several distinct contributions: nonresonant single-parton scattering (NRSPS), double-parton scattering (DPS), combinatorial background (Comb), feed-down, and a near-threshold enhancement represented by BW_0, which is convolved with the detector resolution function R_0. The overall probability density function for the fit can be expressed as

$$\begin{aligned}\mathrm{Model}(m) = {} & N_{\text{interfering BWs}} \cdot \left| r_1 e^{i\phi_1} f_{\mathrm{BW}_1}(m) + f_{\mathrm{BW}_2}(m) + r_3 e^{i\phi_3} f_{\mathrm{BW}_3}(m) \right|^2 \\ & + N_{\mathrm{BW0}} \cdot f_{\mathrm{BW}_0}(m) \otimes R_0(m) + N_{\mathrm{NRSPS}} \cdot f_{\mathrm{NRSPS}}(m) \\ & + N_{\mathrm{DPS}} \cdot f_{\mathrm{DPS}}(m) + N_{\mathrm{Comb.}} \cdot f_{\mathrm{Comb.}}(m) + N_{\text{feed-down}} \cdot f_{\text{feed-down}}(m).\end{aligned} \tag{1}$$

Here, N indicates the yield of each component, while f represents its associated probability density function. The three resonant structures are described using the "three-way" BW interference model already employed in the Run 2 analysis [6], where r_j and ϕ_j are the relative amplitudes and phase angles of $X(6600)$ and $X(7100)$ with respect to $X(6900)$.

The interference fit result for the $J/\psi J/\psi$ mass spectrum is shown in Fig. 1, illustrating the individual components and the total squared amplitude of the interfering BW signals. The fit results of the $J/\psi J/\psi$ interference fit are listed in Table 1. A likelihood-ratio test confirms that all structures have significances exceeding 5σ. In particular, the $X(7100)$ structure has a significance of 7.7σ, surpassing the observation threshold for the first time. The dips near 6750 and 7150 MeV correspond to the $X(6600)$–$X(6900)$ and $X(6900)$–$X(7100)$ interference terms, with significances of 9.7σ and 6.5σ, respectively.

4. CMS $J/\psi\psi(2S)$ analysis with combined Run 2 and Run 3 dataset

As $\psi(2S)$ is the radial excitation of J/ψ , structures corresponding to genuine resonances are expected to decay into $J/\psi\psi(2S)$ final states. The $J/\psi\psi(2S)$ channel is analyzed in the $\mu^+\mu^-\mu^+\mu^-$ decay mode using the combined Run 2 and Run 3 datasets [13]. In the default fit, only $X(6900)$ and $X(7100)$ are included, as $X(6600)$ lies below the kinematic threshold. Following the $J/\psi J/\psi$ model, the $J/\psi\psi(2S)$ mass spectrum (Fig. 1) is fitted with interfering $X(6900)$ and

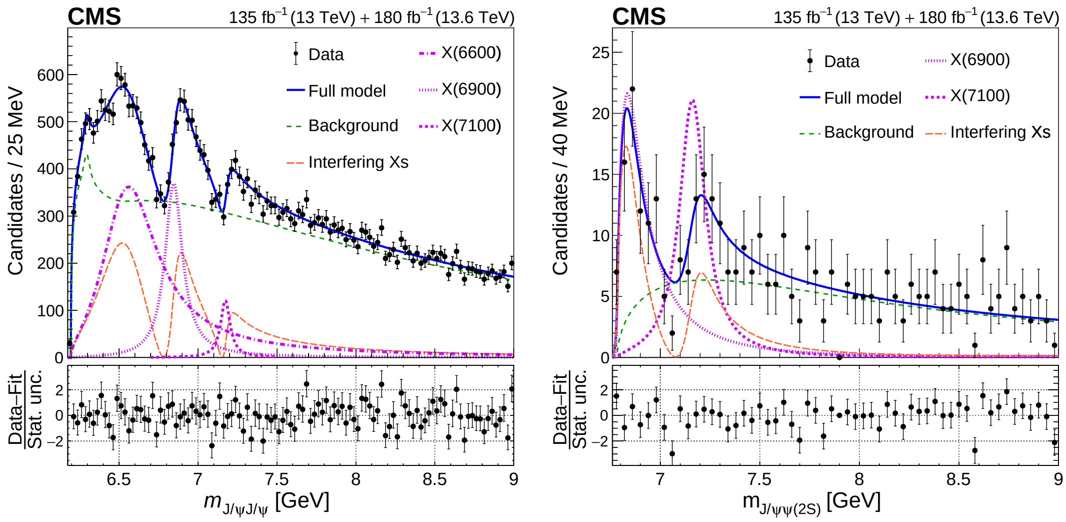

Figure 1: Left: The $J/\psi J/\psi$ invariant-mass spectrum up to 9 GeV. Right: The $J/\psi\psi(2S)$ invariant-mass spectrum up to 9 GeV. The data is fit up to 15 GeV using an unbinned likelihood, with the spectrum binned for display.

$X(7100)$ signals, together with NRSPS, DPS, and combinatorial backgrounds. The fit results are summarized in Table 1. The significances of $X(6900)$ and $X(7100)$ are 8.1σ and 4.3σ, respectively.

Table 1: Summary of fit results for the $X(6600)$, $X(6900)$, and $X(7100)$ states in $J/\psi J/\psi$ and $J/\psi\psi(2S)$ channel. Uncertainties are statistical, followed by systematic.

	$J/\psi J/\psi \to \mu^+\mu^-\mu^+\mu^-$		$J/\psi\psi(2S) \to \mu^+\mu^-\mu^+\mu^-$	
	M [MeV]	Γ [MeV]	M [MeV]	Γ [MeV]
$X(6600)$	$6593^{+15}_{-14} \pm 25$	$446^{+66}_{-54} \pm 87$	–	–
$X(6900)$	$6847^{+10}_{-10} \pm 15$	$135^{+16}_{-14} \pm 14$	$6876^{+46+111}_{-29-112}$	$253^{+290+140}_{-100-134}$
$X(7100)$	$7173^{+9}_{-10} \pm 13$	$73^{+18}_{-15} \pm 10$	7169^{+26+90}_{-52-83}	$154^{+110+140}_{-82-181}$

5. Spin-parity measurement of $J/\psi J/\psi$ structures

The spin-parity of the three tetraquark candidates is studied in the $J/\psi J/\psi \to \mu^+\mu^-\mu^+\mu^-$ channel using the CMS Run 2 dataset [14], applying the same event selection as in Ref. [6]. To minimize model dependence, only the decay angles are utilized.

The analysis considers several spin–parity hypotheses, including spins 0, 1, and 2 with both parities. Instead of performing a multidimensional fit using all decay angles, an optimal discriminant $\mathcal{D}_{ij}$ is defined for each hypothesis pair i and j, based on the likelihood ratio between them [15]. One example of the distribution of $\mathcal{D}_{ij}$ for separating the 2^+_m and 0^- scenarios is shown in Fig. 2 (left), while background distributions, derived from the sideband region, exhibit good agreement between data and simulation, as seen in Fig. 2 (right). To extract the spin-parity information, a two-dimensional likelihood model $\mathcal{P}_{ij}(m_{4\mu}, \mathcal{D}_{ij})$ is constructed, incorporating both the $J/\psi J/\psi$ invariant mass and the discriminant, and is used to fit the data. To compare two spin-parity hypotheses J_i^P and J_j^P, the test statistic is defined as $q = -2\ln(\mathcal{L}_{J_j^P}/\mathcal{L}_{J_i^P})$, where $\mathcal{L}$ represents the likelihood obtained from a two-dimensional fit using $\mathcal{P}_{ij}(m_{4\mu}, \mathcal{D}_{ij})$. This procedure is applied to all pairs among the eight J_i^P models. In every comparison involving the 2_m^+ hypothesis, 2_m^+ consistently emerges as the favored scenario.

The results of these tests are summarized in Fig. 3. Overall, negative-parity assignments are excluded with significance exceeding 3σ, the spin-1^+ hypothesis is disfavored at the 99% confidence level, and spin-0^+ at the 95% confidence level. While higher-spin states cannot be completely ruled out, they are less probable due to their higher energy requirements, making the data most consistent with a spin-2^+ assignment.

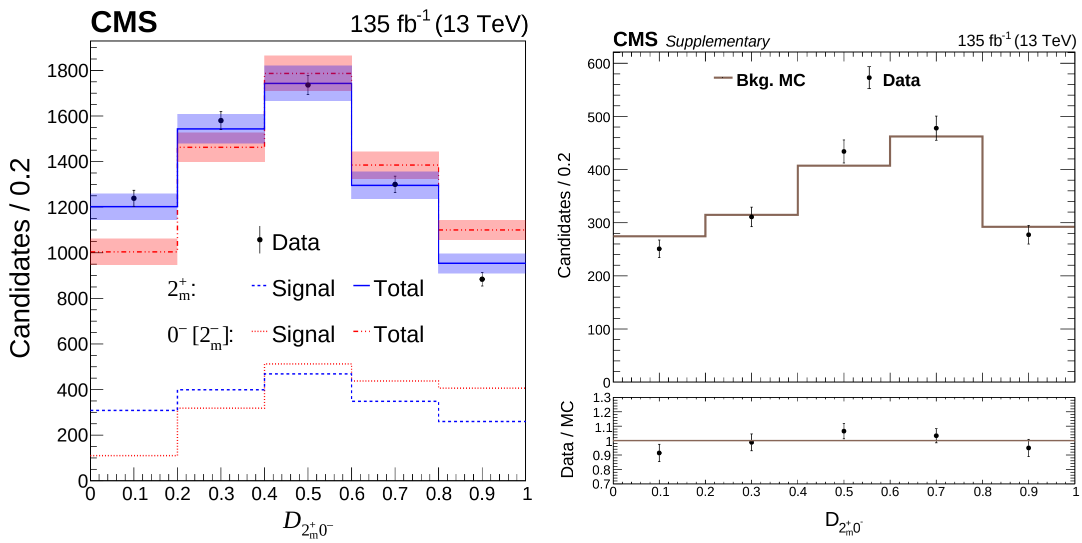

Figure 2: Left: Distribution of the discriminant $\mathcal{D}_{2_m^+0^-}$ used to separate the spin-parity hypotheses 2_m^+ and 0^-. Right: Distributions of the discriminant for background MC and data in the sideband region.

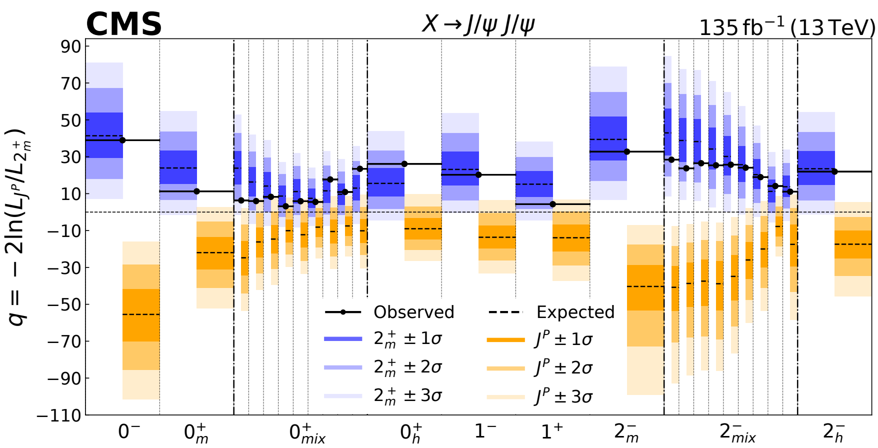

Figure 3: Distributions of the test statistic q for various J_i^P hypotheses tested against the 2_m^+ model.

6. Conclusion

The analysis of the $J/\psi J/\psi$ mass spectrum has been extended with 3.6 times more $J/\psi J/\psi$ pairs, revealing a clear pattern of mutually interfering $X(6600)$, $X(6900)$, and $X(7100)$ structures. The statistical uncertainties on the masses and widths are reduced by a factor of three, owing not only to the enlarged dataset but also to improvements in the fit model. The systematic uncertainties are also reduced by approximately a factor of two. All three states are now firmly established with significances well above 5σ, corroborated by results in the $J/\psi\psi(2S)$ channel, where $X(6900)$ exceeds 5σ and $X(7100)$ reaches 4.3σ. The interference pattern among the three resonances is also statistically compelling, indicating a common J^{PC}. Based on this assumption, a spin-parity analysis using the CMS Run 2 dataset favors a 2^{++} assignment. Future studies, such as exploring additional decay channels and performing cross-section measurements, will be crucial to further elucidate the internal structure of these compelling tetraquark candidates.

References

[1] Murray Gell-Mann. A schematic model of baryons and mesons. *Phys. Lett.*, 8:214, 1964.

[2] G. Zweig. An SU(3) model for strong interaction symmetry and its breaking. Version 2. *CERN*, 1964.

[3] Belle Collaboration. Observation of a narrow charmoniumlike state in exclusive $B^{\pm} \to K^{\pm}\pi^{+}\pi^{-}J/\psi$ decays. *Phys. Rev. Lett.*, 91:262001, 2003.

[4] BESIII Collaboration. Observation of a charged charmoniumlike structure in $e^{+}e^{-} \to \pi^{+}\pi^{-}J/\psi$ at $\sqrt{s} = 4.26$ GeV. *Phys. Rev. Lett.*, 110:252001, 2013.

[5] Belle Collaboration. Observation of a resonance-like structure in the $\pi^{\pm}\psi'$ mass distribution in exclusive $B \to K\pi^{\pm}\psi'$ decays. *Phys. Rev. Lett.*, 100:142001, 2008.

[6] CMS Collaboration. New structures in the $J/\psi J/\psi$ mass spectrum in proton-proton collisions at $\sqrt{s} = 13$ TeV. *Phys. Rev. Lett.*, 132:111901, 2024.

[7] LHCb Collaboration. Observation of structure in the J/ψ-pair mass spectrum. *Sci. Bull.*, 65:1983, 2020.

[8] ATLAS Collaboration. Observation of an excess of dicharmonium events in the four-muon final state with the ATLAS detector. *Phys. Rev. Lett.*, 131:151902, 2023.

[9] ATLAS Collaboration. Observation of structures in the $J/\psi + \psi(2S)$ mass spectrum with the ATLAS detector. To appear in *Phys. Rev. Lett.*, 2025.

[10] Feng Zhu, Gerry Bauer, and Kai Yi. Experimental road to a charming family of tetraquarks . . . and beyond. *Chin. Phys. Lett.*, 41:111201, 2024.

[11] CMS Collaboration. Observation of a family of all-charm tetraquark candidates at the LHC. Technical report, CERN, Geneva, 2025.

[12] Aram Hayrapetyan et al. Enriching the physics program of the CMS experiment via data scouting and data parking. *Phys. Rept.*, 1115:678, 2025.

[13] CMS Collaboration. Observation of X(6900) and evidence of X(7100) in the psi(2S)Jpsi to 4mu mass spectrum in pp collisions at CMS. Technical report, CERN, Geneva, 2025.

[14] CMS Collaboration. Determination of the spin and parity of all-charm tetraquarks. *Nature*, 648:58, 2025.

[15] Yanyan Gao, Andrei V. Gritsan, Zijin Guo, Kirill Melnikov, Markus Schulze, and Nhan V. Tran. Spin determination of single-produced resonances at hadron colliders. *Phys. Rev. D*, 81:075022, 2010.

PoS(HQL2025)050